

## Effective Atherosclerotic Plaque Inflammation Inhibition with Targeted Drug Delivery by Hyaluronan Conjugated Atorvastatin Nanoparticles

Syedmehdi Hossaini Nasr,<sup>a,b</sup>& Zahra Rashidijahanabad,<sup>a,b</sup>& Sherif Ramadan,<sup>a,b,c</sup> Nate Kauffman,<sup>b,d</sup> Narayanan Parameswaran,<sup>e</sup> Kurt R. Zinn,<sup>b,d,f</sup> Chunqi Qian,<sup>f</sup> Ripla Arora,<sup>b,g</sup> Dalen Agnew,<sup>h</sup> Xuefei Huang<sup>a,b,d\*</sup>

<sup>a</sup>Department of Chemistry, <sup>b</sup>Institute for Quantitative Health Science and Engineering, <sup>d</sup>Department of Biomedical Engineering, <sup>e</sup>Department of Physiology, <sup>f</sup>Department of Radiology, <sup>g</sup>Department of Obstetrics, Gynecology and Reproductive Biology, and <sup>h</sup>Department of Pathobiology and Diagnostic Investigation, Michigan State University, East Lansing, Michigan 48824, USA

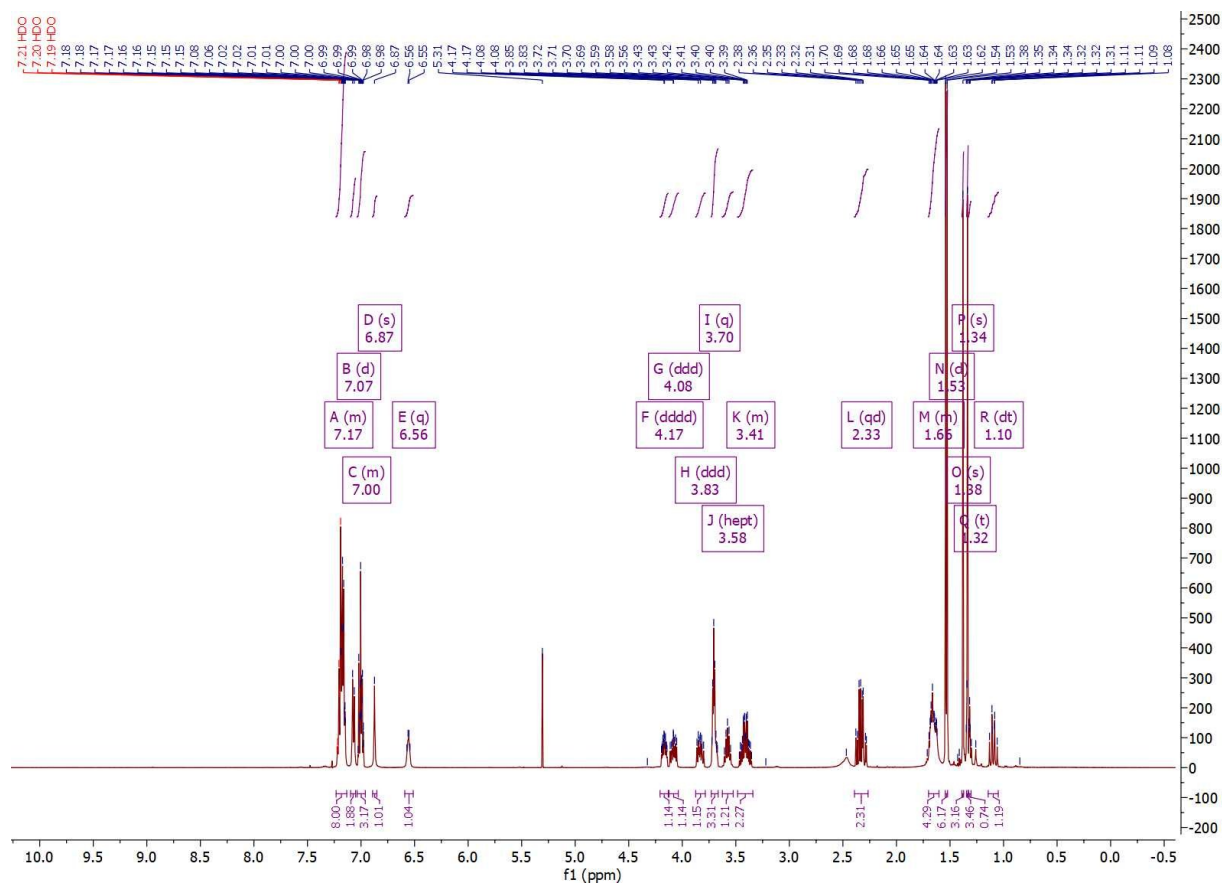
<sup>c</sup>Chemistry Department, Faculty of Science, Benha University, Benha, Qaliobiya 13518, Egypt

Email: huangxu2@msu.edu

\*Equal contribution to the work.

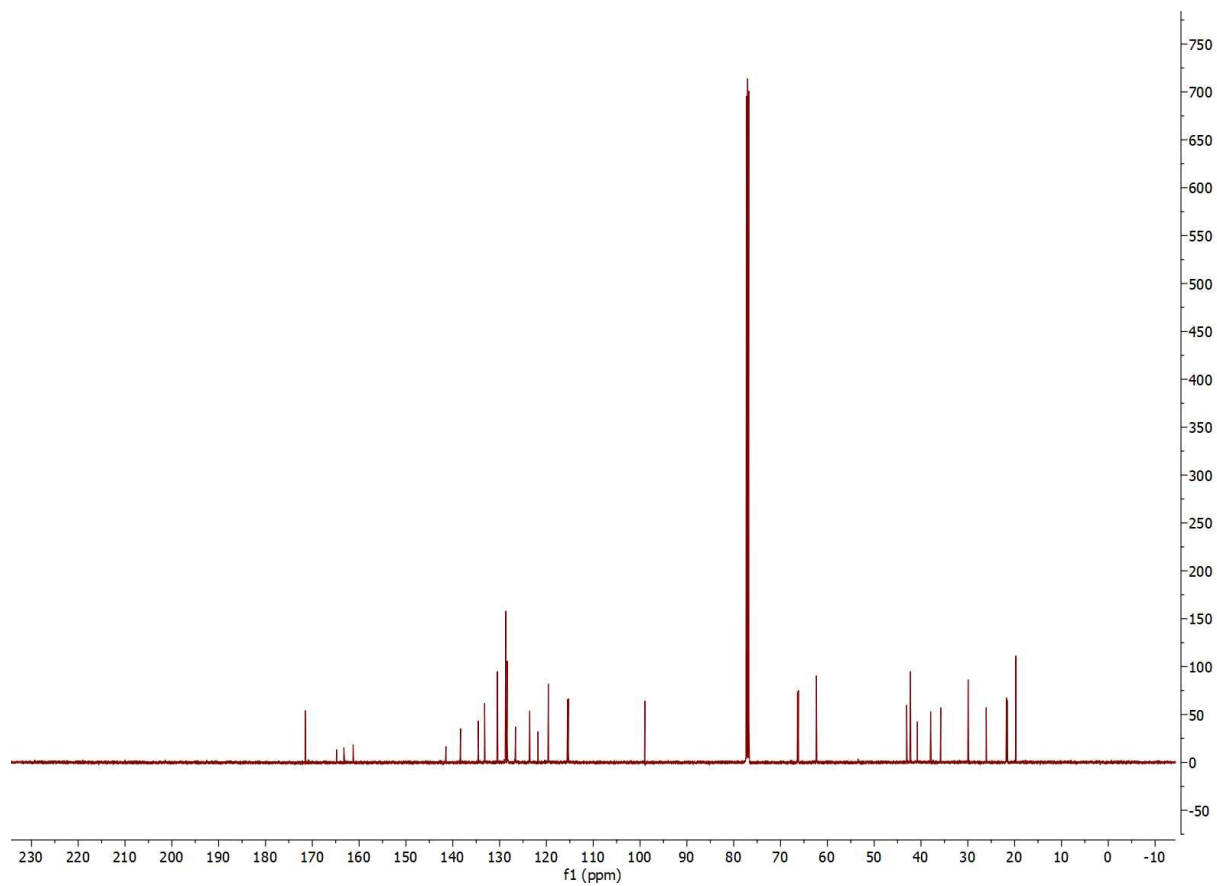
## Table of Contents

Figure S1. <sup>1</sup> H-NMR spectrum of atorvastatin-linker (Compound 7)	S3
Figure S2. <sup>13</sup> C-NMR spectrum of atorvastatin-linker (Compound 7)	S4
Figure S3. g-COSY spectrum of atorvastatin-linker (Compound 7)	S5
Figure S4. ESI mass spectrum of atorvastatin-linker (Compound 7)	S6
Figure S5. <sup>1</sup> H-NMR spectrum of HA-ATV conjugate in DMSO-d <sub>6</sub> .	S7
Figure S6. Agarose gel electrophoresis for free HA and HA-ATV conjugate	S8
Figure S7. <sup>1</sup> H-NMR spectrum of HA-ATV conjugate in D <sub>2</sub> O.	S9
Figure S8. Size and zeta potential of HA-ATV NP prepared in water on days 1, 14 and 34.	S9
Figure S9. Size and zeta potential of freeze-dried HA-ATV NP.	S10
Figure S10. Atorvastatin release curve from HA-ATV NP.	S11
Figure S11. Isopropylidene removal from compound 4 at pH 5.	S12
Scheme S1. Formation of phenanthrene ring in ATV after UV irradiation.	S13
Figure S12. Confocal imaging of atorvastatin in RAW264.7 cells.	S13
Figure S13. <sup>19</sup> F-NMR spectra of RAW264.7 cell lysate after incubation with (a) HA-ATV NP and (b) free ATV	S14
Figure S14. rt-PCR analysis of RAW264.7 cells with various treatments.	S15
Figure S15. MRI images of control group ApoE knockout mice aorta at week 6 and week 7 after high fat diet. This group did not receive HA-ATV NP during week 7.	S16
Figure S16. Histology analysis of aortas.	S17
Figure S17. rt-PCR analysis of RAW264.7 cells treated with a mixture of free HA and ATV.	S18
Figure S18. ZetaView <sup>®</sup> analysis of HA-ATV NP in different dilutions.	S19
Figure S19. Confocal images of RAW264.7 cells incubated with FITC HA-ATV NPs.	S20
Figure S20. Biodistribution study of HA-ATV NP.	S21
References	S21



**Figure S1.**  $^1\text{H}$ -NMR spectrum of atorvastatin amine derivative **7**.

$^1\text{H}$  NMR (500 MHz, Chloroform-*d*)  $\delta$  7.23 – 7.13 (m, 8H), 7.07 (d,  $J$  = 8.0 Hz, 2H), 7.04 – 6.96 (m, 3H), 6.87 (s, 1H), 6.56 (q,  $J$  = 5.1 Hz, 1H), 4.17 (dddd,  $J$  = 11.7, 7.2, 4.3, 2.5 Hz, 1H), 4.08 (ddd,  $J$  = 14.5, 9.8, 6.0 Hz, 1H), 3.83 (ddd,  $J$  = 14.5, 9.7, 6.6 Hz, 1H), 3.70 (q,  $J$  = 5.1 Hz, 3H), 3.58 (hept,  $J$  = 7.1 Hz, 1H), 3.48 – 3.34 (m, 2H), 2.33 (qd,  $J$  = 14.9, 5.9 Hz, 2H), 1.70 – 1.60 (m, 4H), 1.53 (d,  $J$  = 7.1 Hz, 6H), 1.38 (s, 3H), 1.34 (s, 3H), 1.32 (t,  $J$  = 2.5 Hz, 1H), 1.10 (dt,  $J$  = 12.9, 11.6 Hz, 1H).



**Figure S2.**  $^{13}\text{C}$ -NMR spectrum of atorvastatin amine derivative **7**.

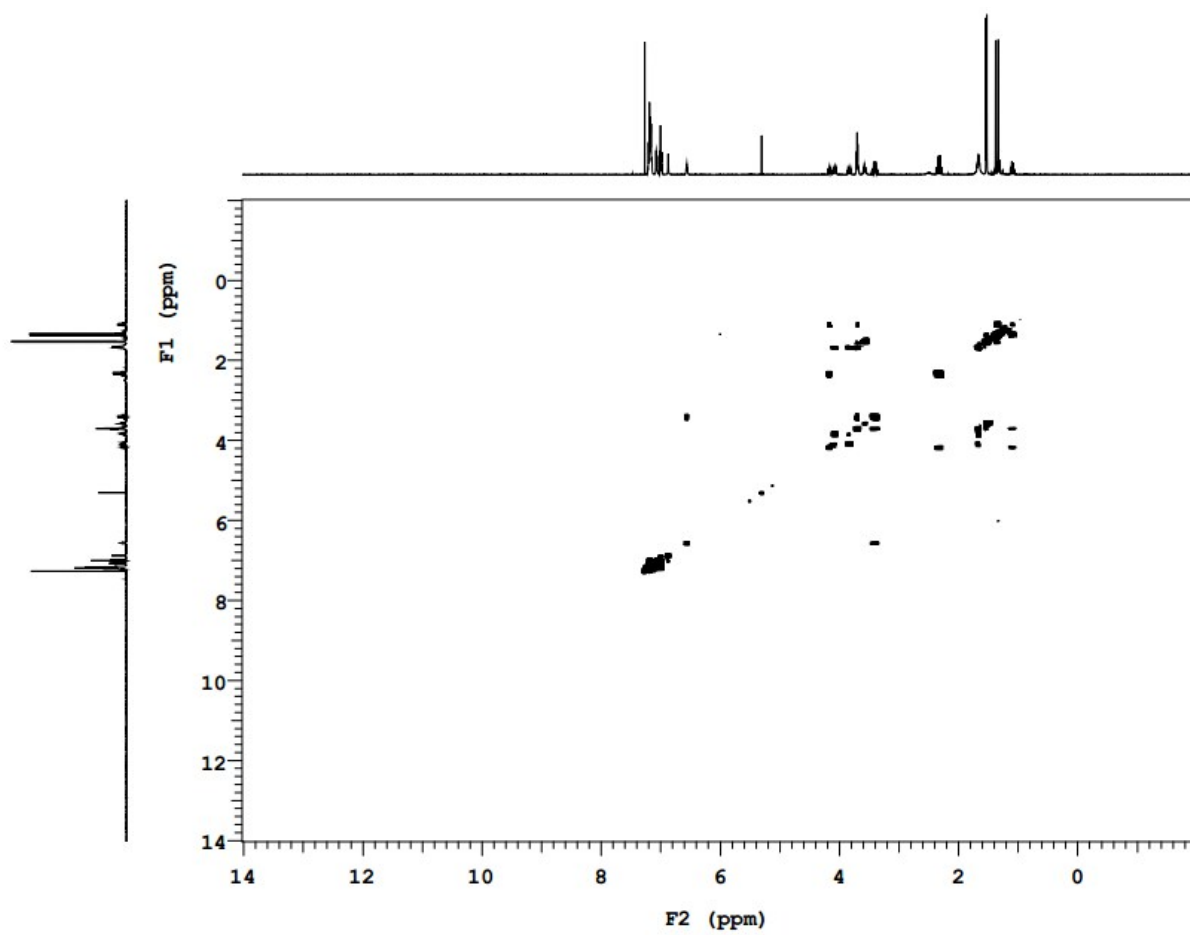


**Figure S3.** G-COSY spectrum of atorvastatin amine derivative 7.

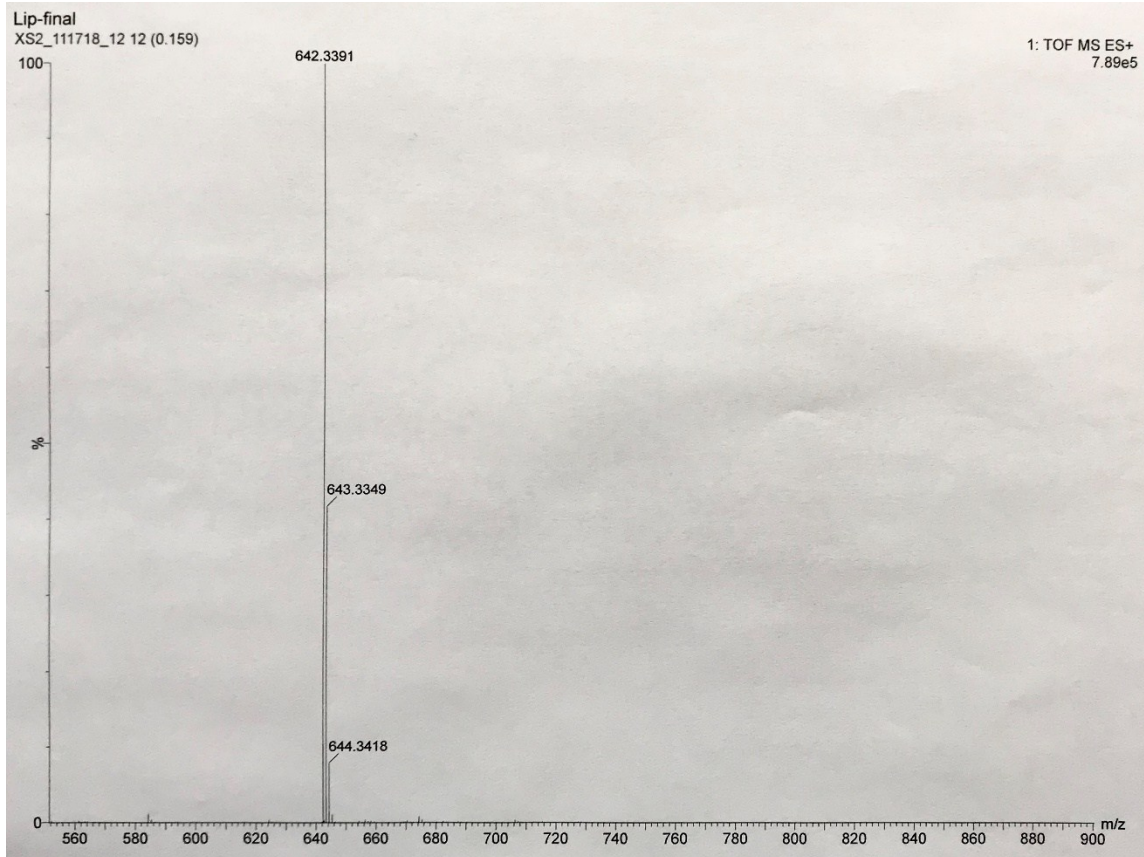


**Figure S4.** ESI mass of atorvastatin amine derivative **7**.

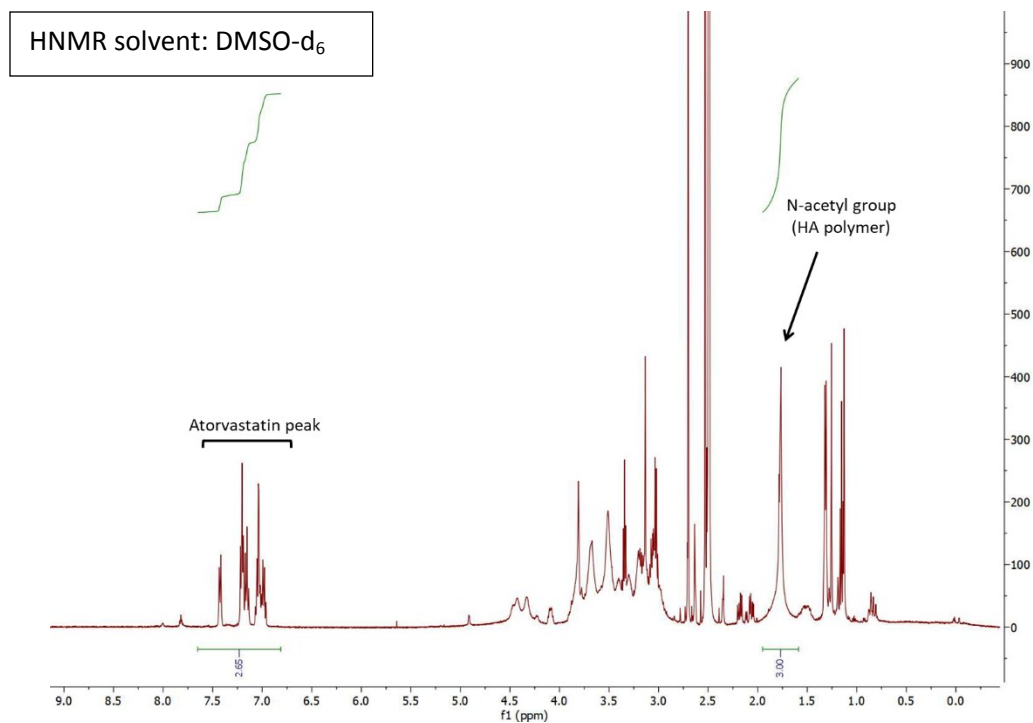


**Figure S5.** <sup>1</sup>H-NMR of HA-ATV conjugate in DMSO-d<sub>6</sub>. By comparing the ratio of integration of aromatic signals (from ATV) and that of the *N*-acetyl group (from HA), the average number of ATV per HA disaccharide was determined to be 0.4, which corresponded to 35% w/w of the total mass of conjugate being ATV.

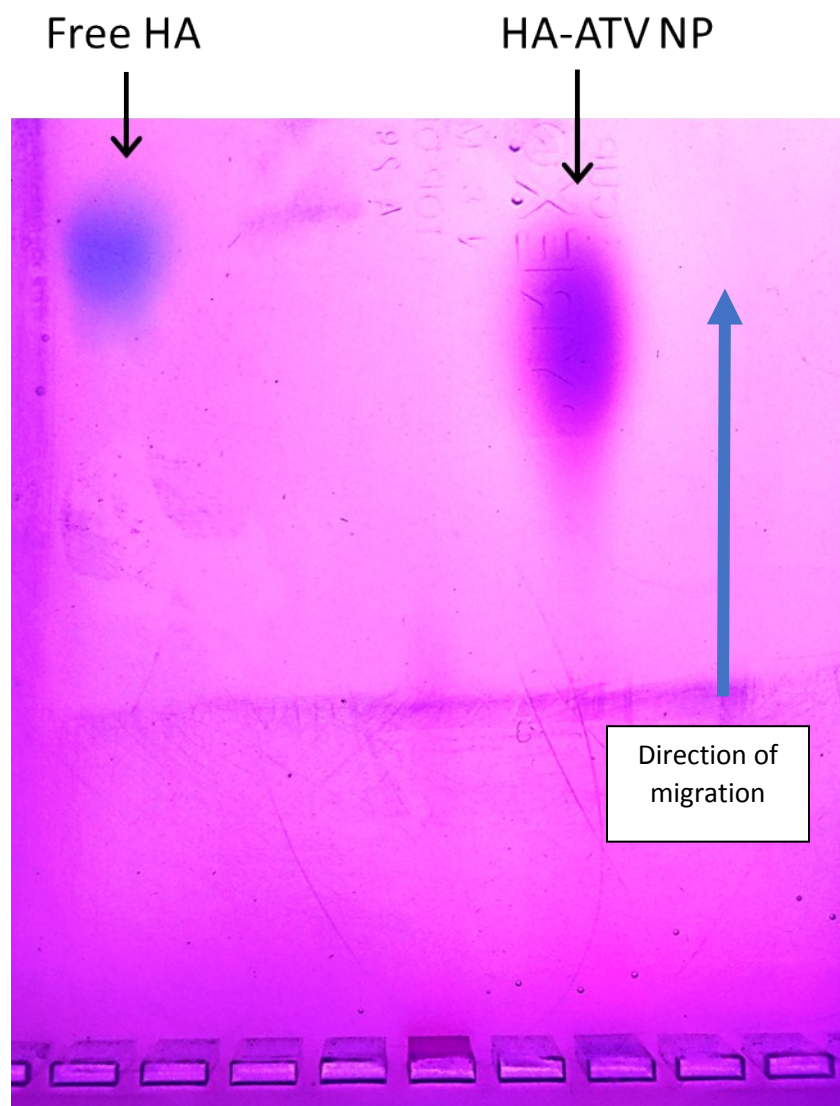


**Figure S6.** Agarose gel electrophoresis for free HA and HA-ATV conjugate. Free HA and HA-ATV conjugate were run on an agarose gel (0.8%) and stained with Stains-All dye. Free HA has a blue color in this staining and HA-ATV conjugate shows up purple. The pore sizes for agarose gel (1%) have been estimated between 100-500 nm<sup>1, 2</sup>. Therefore, it is expected that HA-ATV can move through the gel.

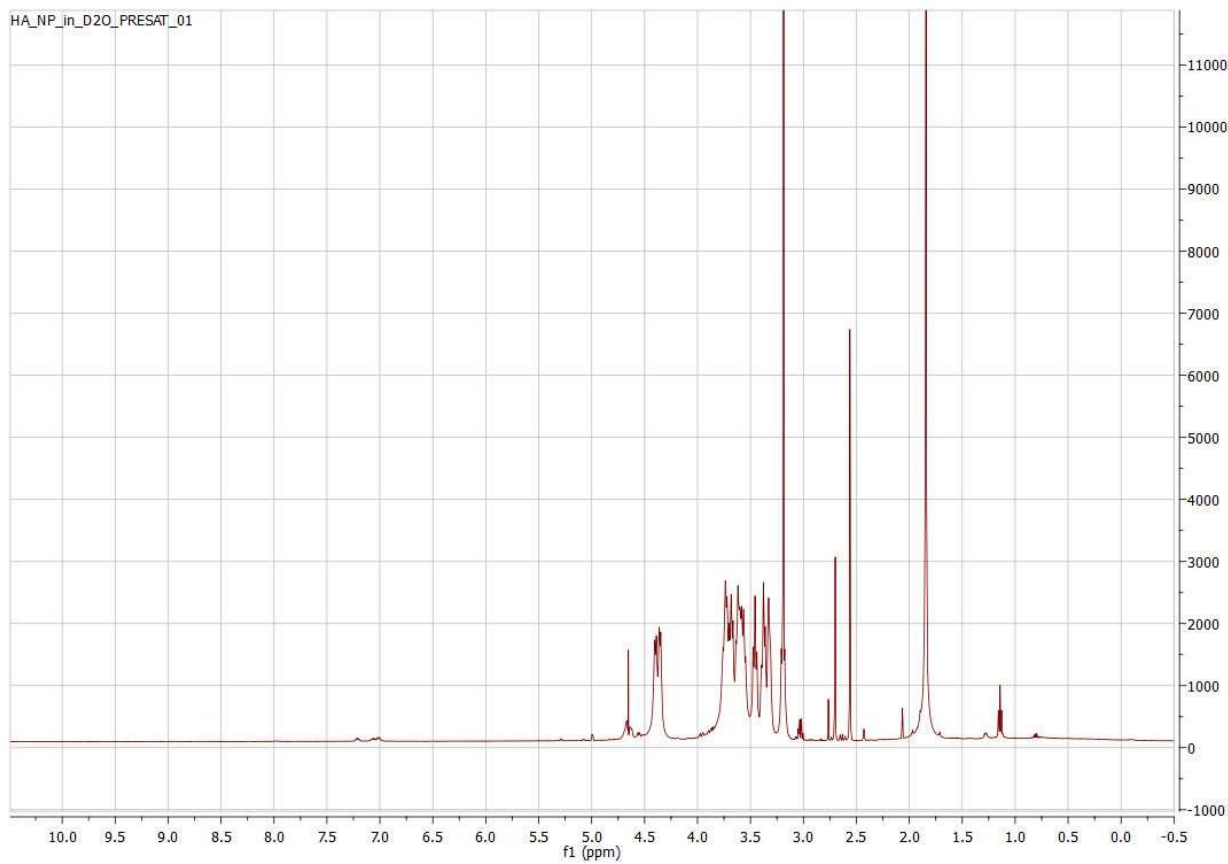


**Figure S7.**  $^1\text{H-NMR}$  spectrum of HA-ATV conjugate in  $\text{D}_2\text{O}$ .

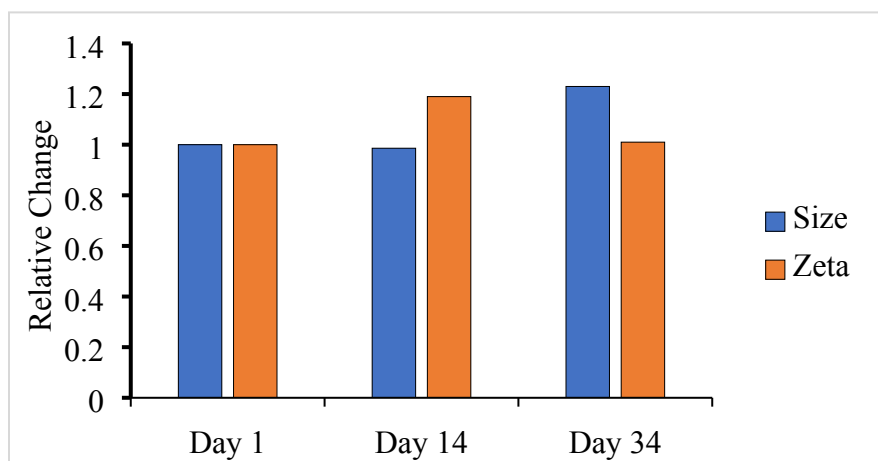


**Figure S8.** Comparison of hydrodynamic diameter and zeta potential of HA-ATV NP prepared in water on days 1, 14 and 34. Relative changes were calculated by dividing the values of hydrodynamic diameter and zeta potential on days 14 and 34 by those on day 1.

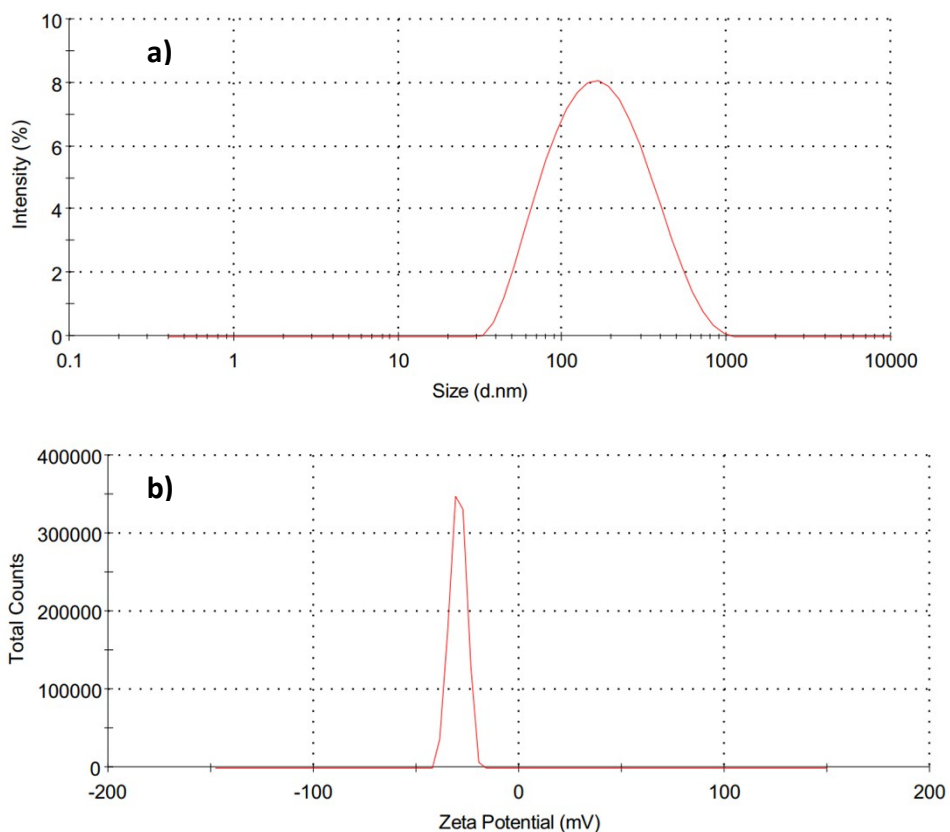


**Figure S9.** Size and zeta potential of freeze-dried HA-ATV NP as determined by DLS. HA-ATV NP prepared in water were freeze-dried and stored at  $-20\text{ }^{\circ}\text{C}$  for 5 months. Then, to this freeze-dried powder, distilled water was added and NPs were re-dispersed after 2-3 times of pipetting. (a) Hydrodynamic diameter of the HA-ATV NPs. The average diameters of regenerated HA-ATV NP were 137 nm. (b) Zeta potential of the HA-ATV NP. The zeta potential of regenerated HA-ATV NP was  $-37\text{ mV}$ . Both hydrodynamic diameter and zeta potential values were similar to those of freshly prepared NPs.

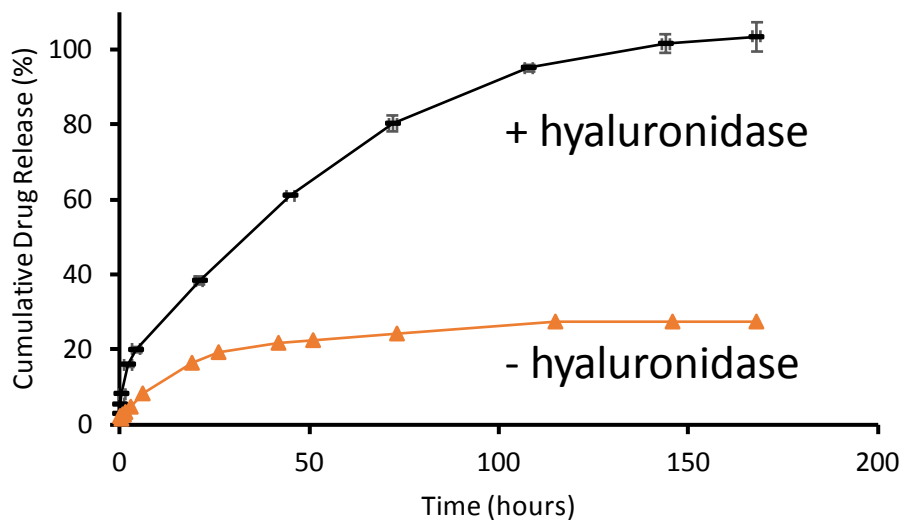


**Figure S10.** ATV could be released from HA-ATV NP upon hyaluronidase (HAase) treatment, while without HAase, much slower release was observed suggesting HAase is critical for high rate of ATV release from HA-ATV NP. Solutions of HA-ATV NPs in pH 7.4 PBS buffer were treated with (0.55 mg/mL) or without a HAase and the amounts of free ATV in the solution were quantified by UV absorbance. The percentages of free ATV released in solution were calculated by dividing the amounts of ATV released over the total amounts of ATV encapsulated.

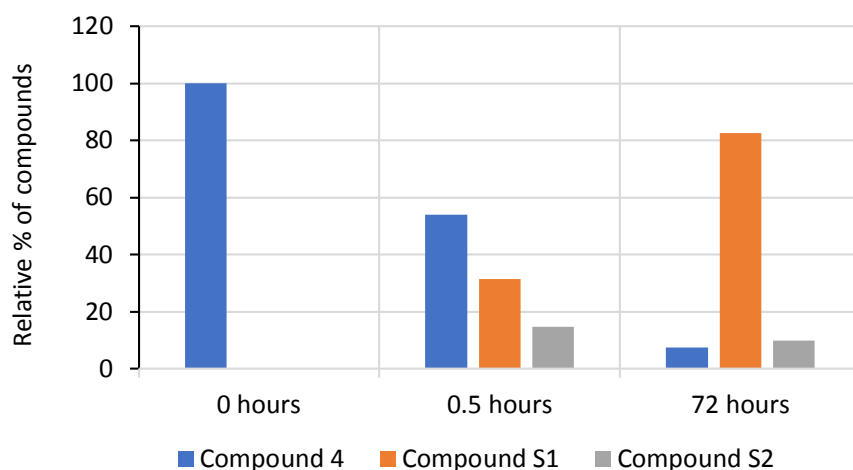
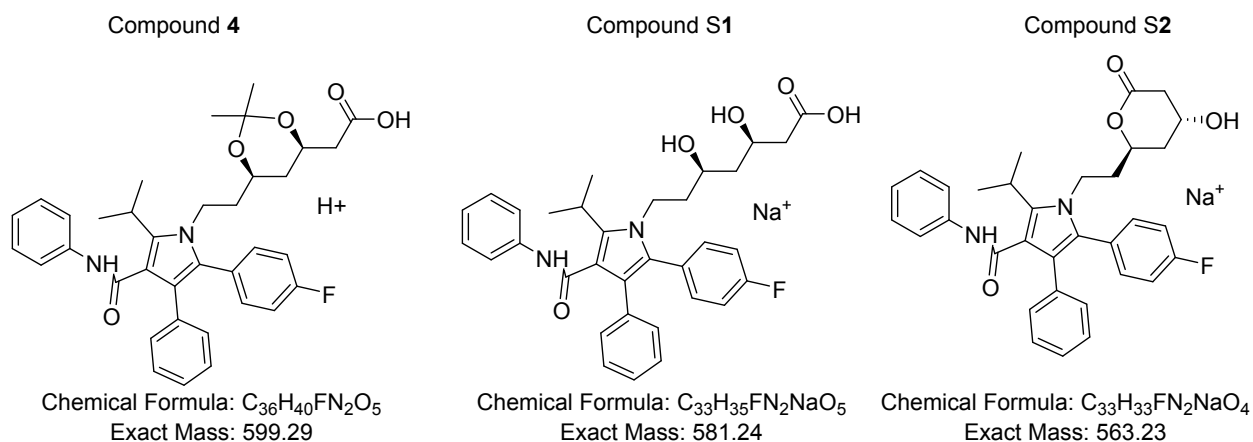
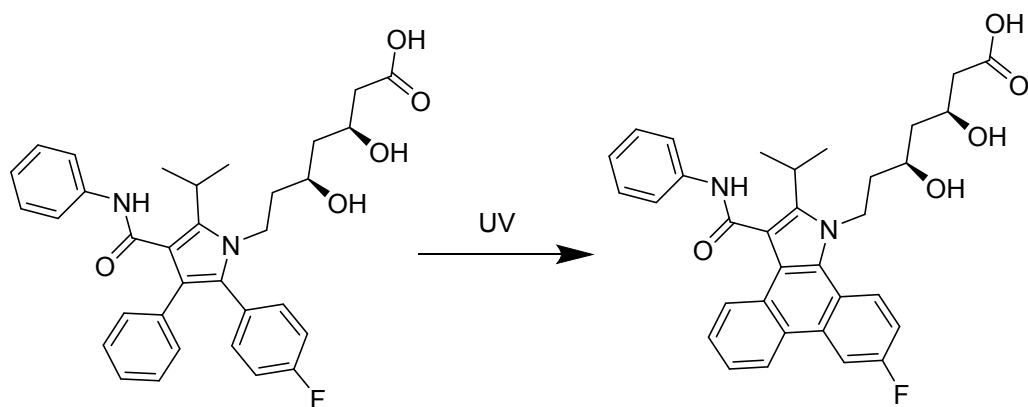


**Figure S11.** Isopropylidene group was removed from ATV derivative **4** at pH 5 suggesting ATV could be unmasked at. Compound **4** was dissolved in pH 5 buffer. The ESI mass spectra of the solution were measured 0.5 hour and 72 hours later. Besides the MS peak corresponding to compound **4** ( $m/z$  599.29), 2 other major peaks were observed in mass spectrum. The peaks at  $m/z=581$  and 563 correspond to free  $ATV+Na^+$  (compound S1) and the lactone form of  $ATV+Na^+$  (compound S2) following removal of the isopropylidene group from **4**. The relative intensities of  $m/z=581$  and 563 peaks increased over  $m/z=599$  over 3-day incubation at pH 5 indicating compound **4** was hydrolyzed under this condition.



**Scheme S1.** Formation of phenanthrene ring in ATV after UV irradiation.

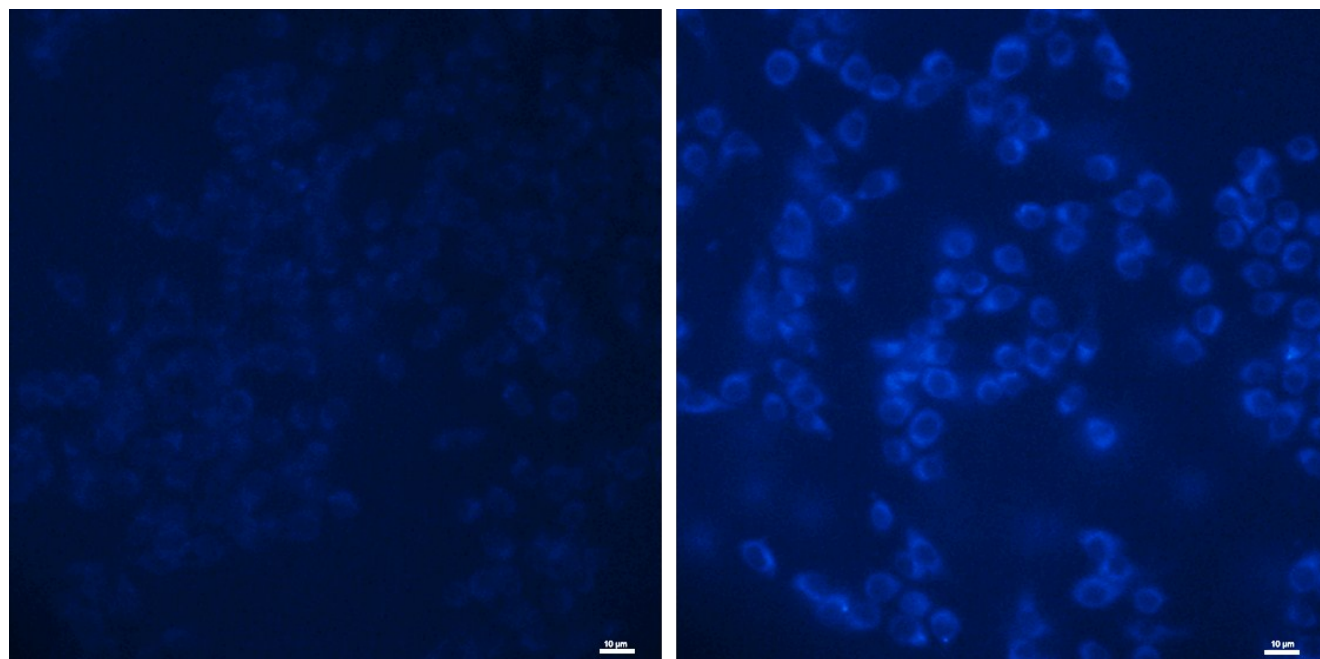


**Figure S12.** Confocal imaging of atorvastatin in RAW264.7 cells. RAW264.7 cells had been incubated with UV irradiated HA-ATV NP and images were collected by confocal microscopy (right image). The left image was for RAW264.7 cells only. The significant increase in blue color (right image) indicates the presence of ATV in the cells. Scale bars are 10 µm.

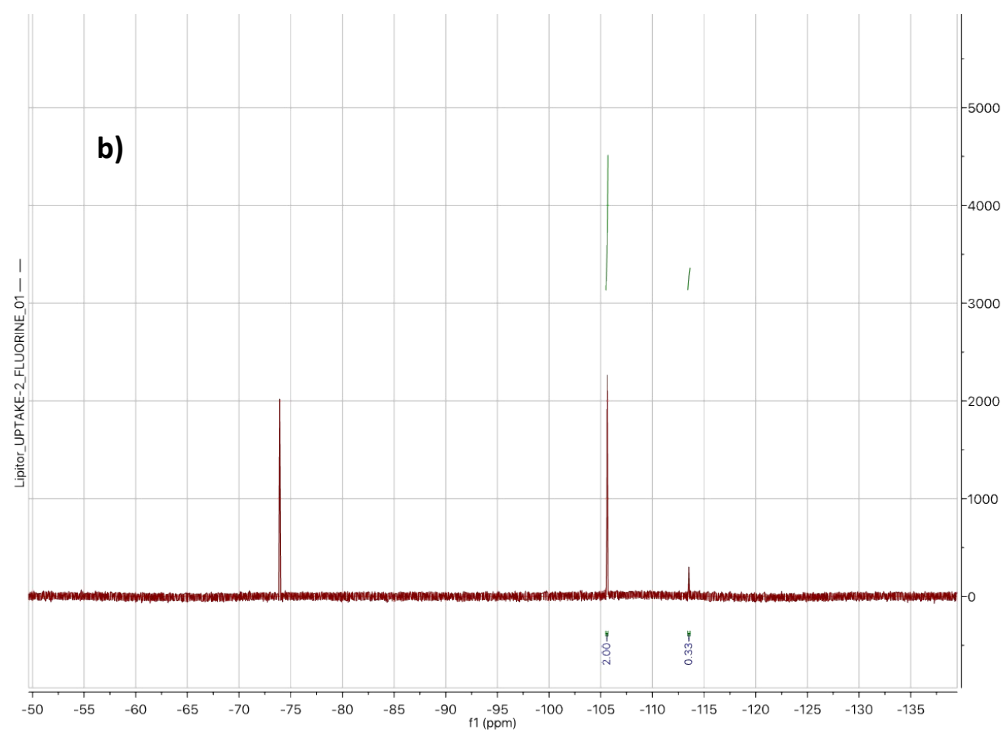
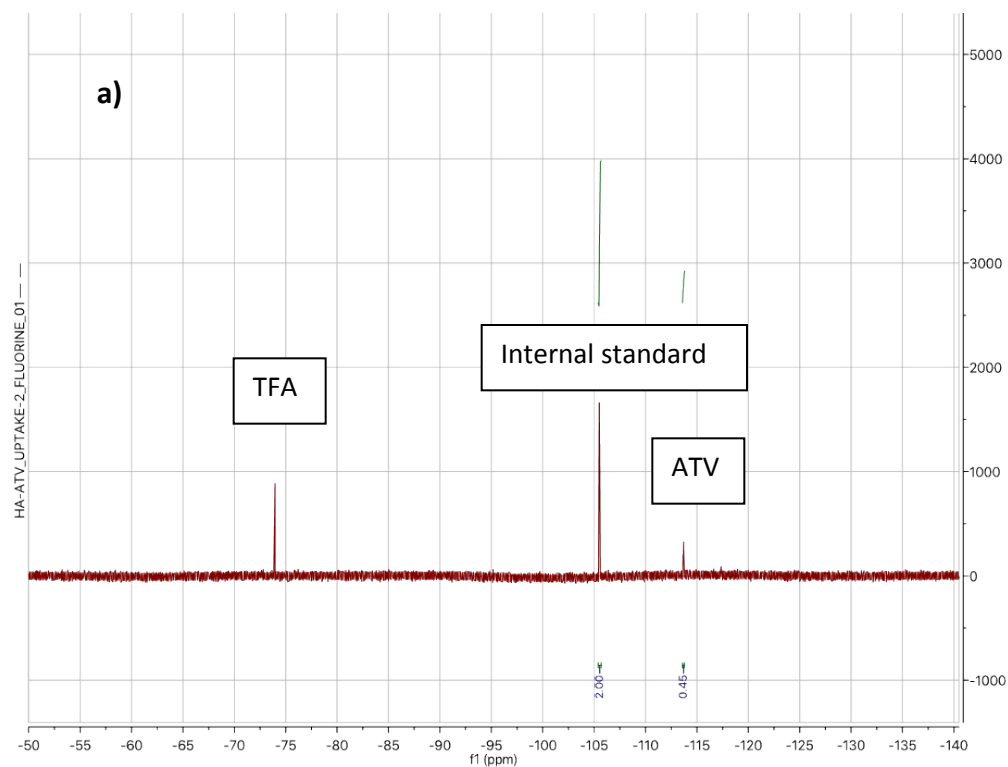


**Figure S13.**  $^{19}\text{F}$ -NMR spectra of RAW264.7 cells after incubation with (a) HA-ATV NP and (b) ATV as free drug. The peaks at -114, -106 and -74 ppm are from ATV, internal standard (4,4'-difluorobenzophenone) and TFA respectively.

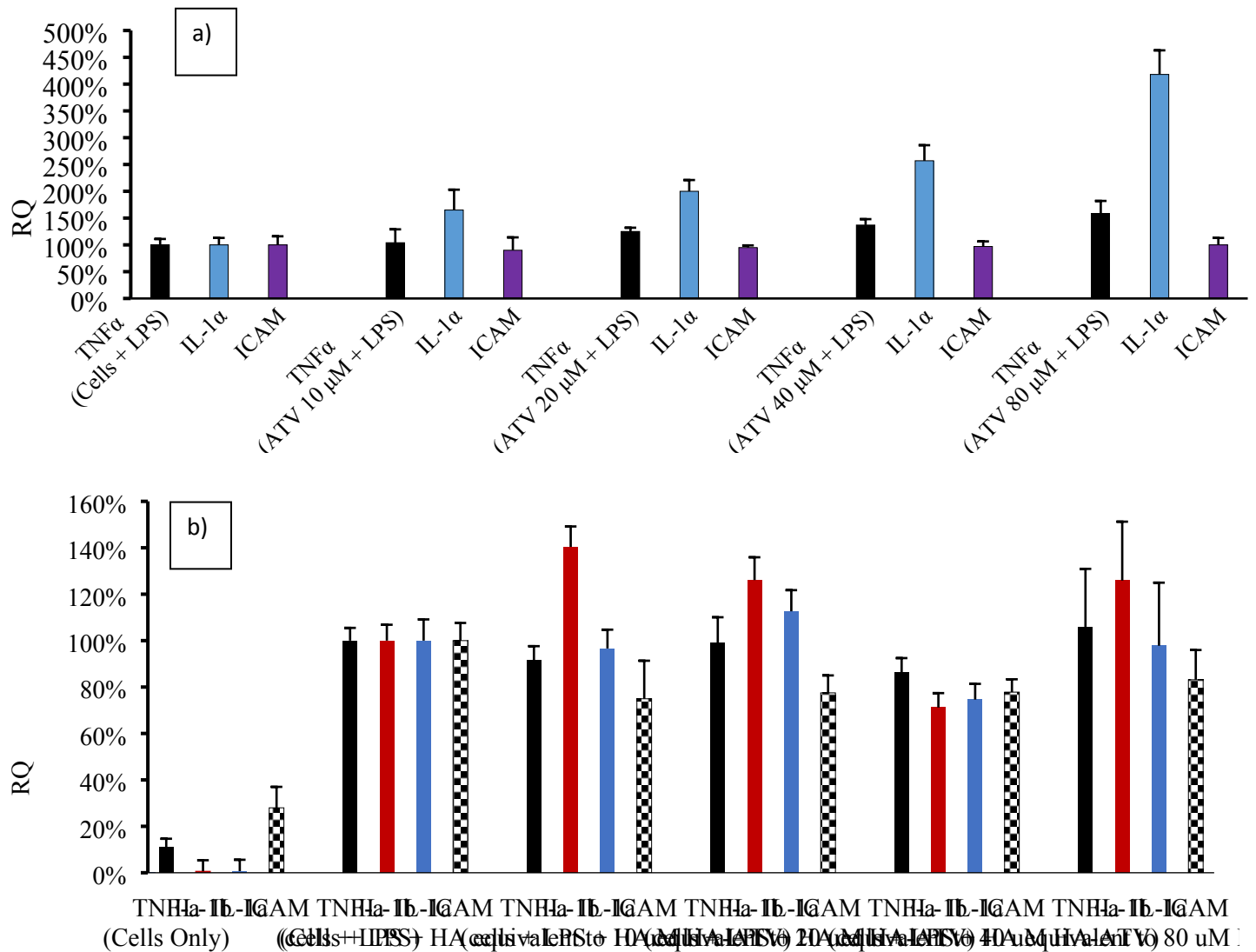


**Figure S14.** rt-PCR analysis of inflammatory cytokines secreted by RAW264.7 cells treated with a) LPS and ATV; and b) LPS and free HA. **ATV or free HA did not show anti-inflammatory effects.** RAW264.7 cells were treated with increasing doses of ATV or free HA for 15 hours and LPS was added with further incubation for another 4 hours. The expression levels of inflammatory genes were analyzed using rt-PCR. No significant reductions of inflammatory cytokines were observed under the conditions evaluated.

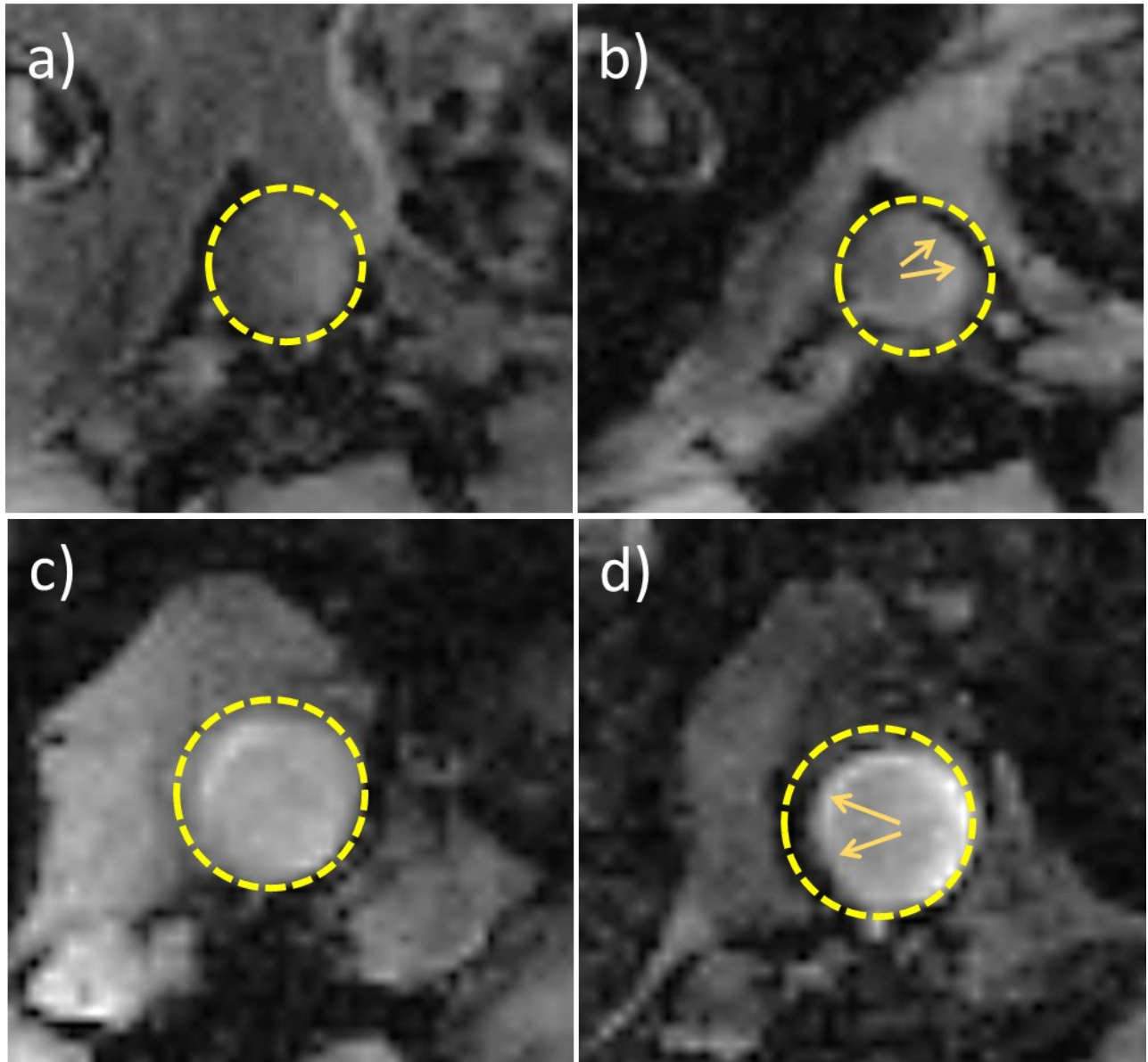


**Figure S15.** T2\* weighted MRI images of control group ApoE knockout mouse aorta at week 6 and week 7 after high fat diet. This group did not receive HA-ATV NP during week 7. Atherosclerotic plaques were detectable in control group in weeks 6 and 7 after high fat diet. (a) and (b) are ApoE knockout mouse aorta 6 weeks after high fat diet. (a) and (b) are MRI images before and after HA-NW injection, respectively. Arrows show the presence of plaques. (c) and (d) are MRI images one week later after receiving PBS buffer. (c) and (d) are MRI images before and after injection of MRI probe (HA-NW) respectively.

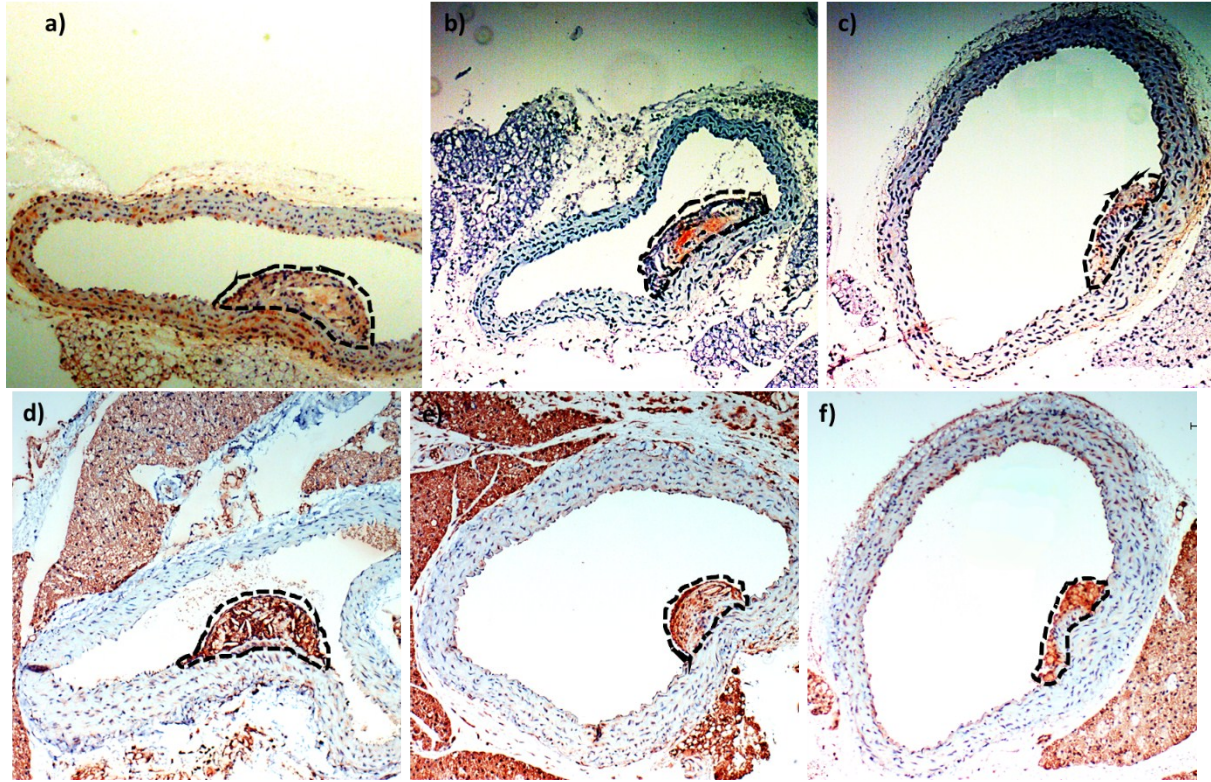


**Figure S16.** Histology study shows macrophage and CD44 reduction after HA-ATV NP treatment. F4/80 staining shows the presence of macrophages in atherosclerotic plaques in (a) control ApoE knockout mouse aorta, (b) ATV treated ApoE knockout mouse aorta and (c) HA-ATV treated ApoE knockout mouse aorta. CD44 staining shows the expression of CD44 receptor in atherosclerotic plaques in (d) control ApoE knockout mouse aorta, (e) ATV treated ApoE knockout mouse aorta and (f) HA-ATV treated ApoE knockout mouse aorta. The borders of plaques are highlighted by dashed lines. The less intense brown stains in plaques areas in c) and f) compared to those in a) and d) suggest the reduction of levels of macrophages and CD44 in plaques.

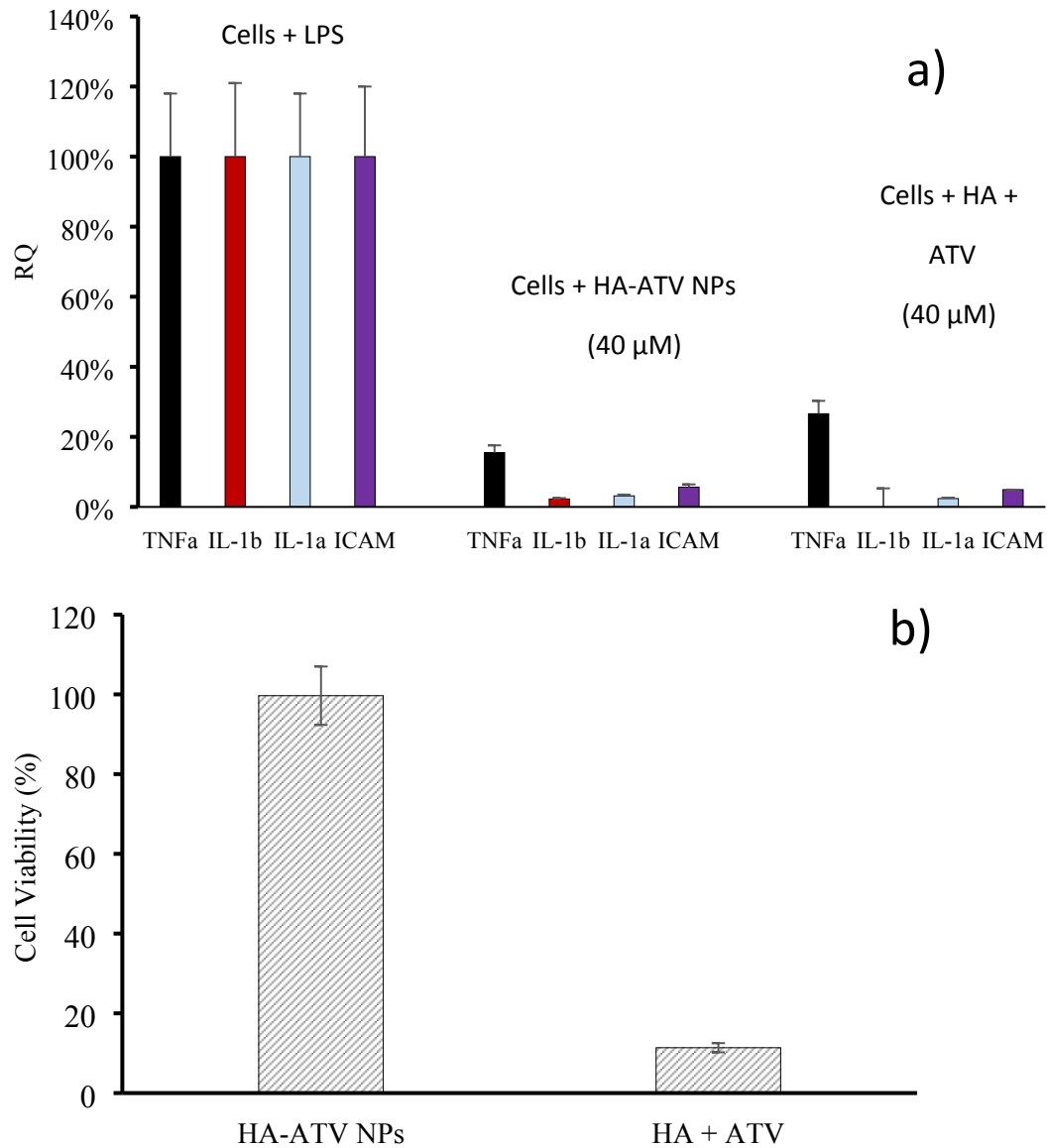


**Figure S17.** (a) rt-PCR analysis of inflammatory cytokines secreted by RAW264.7 cells treated with LPS and a mixture of free HA and ATV for 19 hours. HA-ATV NP was used as a control and the results showed similar anti-inflammatory effect for the mixture of free HA and ATV. (b) RAW264.7 cells were treated with HA-ATV NPs (40 μM) or a mixture of free HA and ATV (HA+ATV 40 μM). Then, cellular viability was measured by cell counting. Cells treated with HA + ATV showed significantly lower cell viability compared to those with HA-ATV NPs.

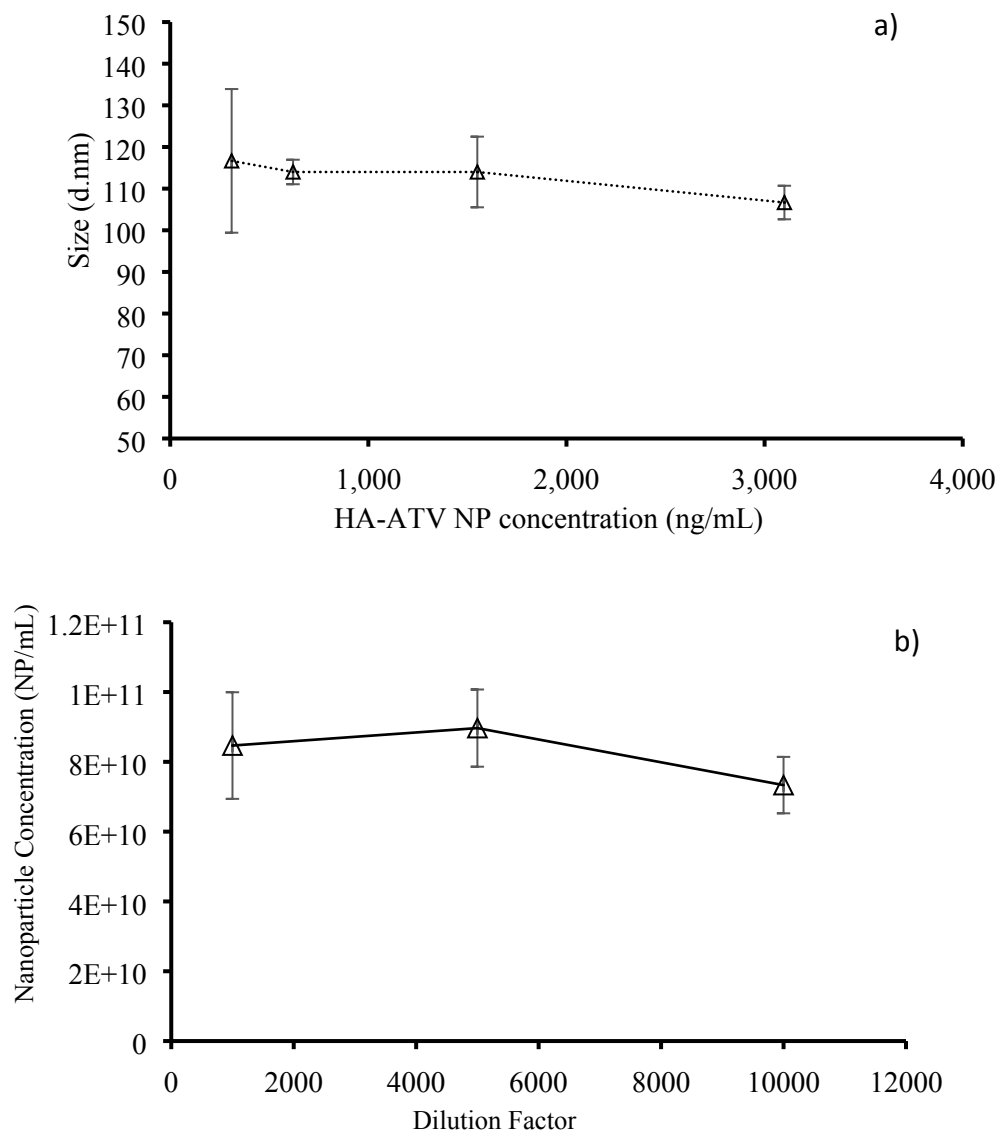


**Figure S18. (a)** HA-ATV NP was diluted in PBS buffer and the size of nanoparticles were monitored. The results suggested that by diluting the sample up to 10,000 folds still the size of nanoparticles do not show significant changes. **(b)** HA-ATV NPs were diluted up to 10000 folds and the concentration of NPs were plotted for different dilution factor (For each dilution data point the NP concentration was multiply by the dilution factor to normalize the final concentration). No significant change in NP concentration was observed after diluting the sample indicating that HA-ATV NPs retain their form even in very low concentrations.

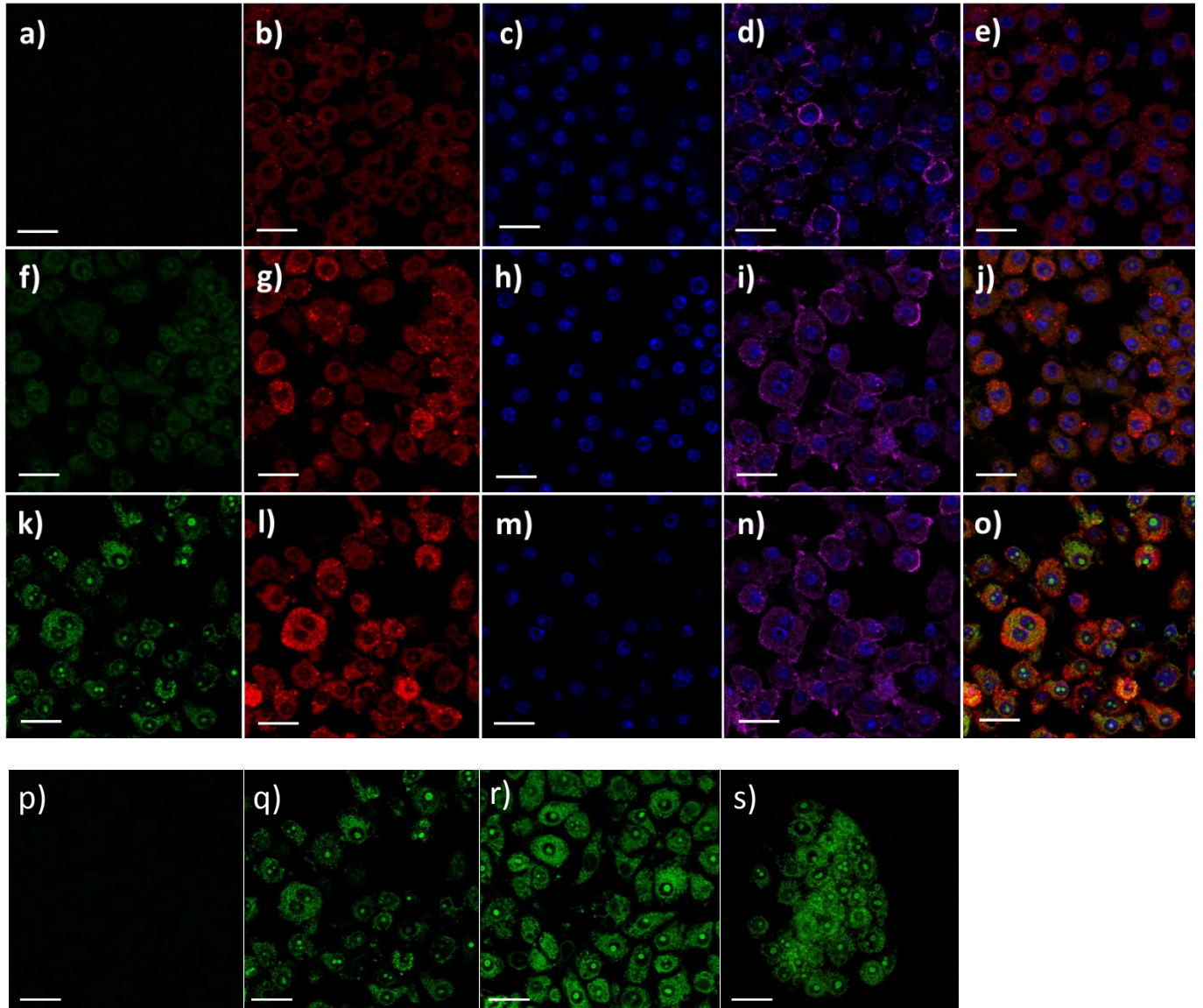


**Figure S19.** Confocal images of RAW264.7 cells incubated with FITC HA-ATV NPs. (a-e) are control cells, (f-j) are cells treated with FITC HA-ATV NPs following 2 h incubation at 4 °C. (k-o) are cells treated with FITC HA-ATV NPs following 2 h incubation at 37 °C. Scale bar is 20  $\mu\text{m}$ . (a, f and k: FITC channel), (b, g and l: red Lysotracker channel), (c, h and m: DAPI channel), (d, i and n: overlay of DAPI and APC anti-CD44 mAb channels), (e, j and o: overlays of FITC, DAPI and Lysotracker channels). (p-s) RAW264.7 cells were treated with FITC HA-ATV NPs and imaged at different time intervals (2, 8 and 24 h). An increase of fluorescence intensities in cells was observed by increasing the incubation time (p: no NP, q, r and s are at 2, 8 and 24 h respectively after NP incubation). Scale bar is 20  $\mu\text{m}$ .

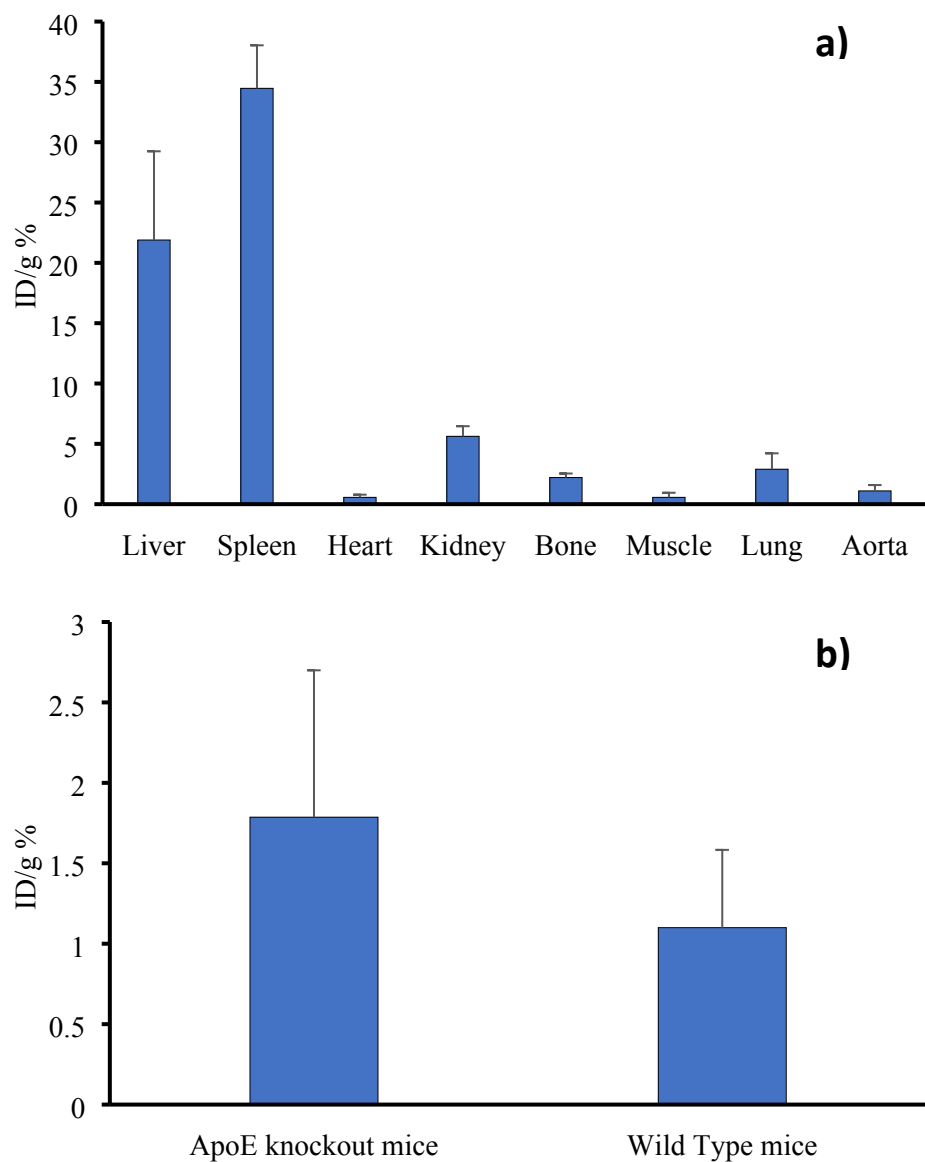


**Figure S20.** Biodistribution study of HA-ATV NP. (a) Mice were injected with  $^{99m}\text{Tc}$  labeled HA-ATV NP and organs radioactivity have been presented based on injected dose per gram animal tissue. Spleen and liver showed the highest uptake. (b) ApoE knockout mice aorta showed higher radioactivity due to higher accumulation of  $^{99m}\text{Tc}$  labeled HA-ATV NP compared to wild type mice aorta.

#### References:

1. B. H. Zimm and S. D. Levene, Problems and prospects in the theory of gel electrophoresis of DNA, *Quarterly Reviews of Biophysics*, 1992, 25, 171-204.
2. J.-L. Viovy, Electrophoresis of DNA and other polyelectrolytes: Physical mechanisms, *Reviews of Modern Physics*, 2000, 72, 813-872.